

Tunable Emissive Lanthanidomesogen Derived from a Room-Temperature Liquid-Crystalline Schiff-Base Ligand

Harun A. R. Pramanik,^[a] Gobinda Das,^[a] Chira R. Bhattacharjee,*^[a] Pradip C. Paul,^[a] Paritosh Mondal,^[a] S. Krishna Prasad,^[b] and D. S. Shankar Rao^[b]

Abstract: A novel photoluminescent room-temperature liquid-crystalline salicylaldimine Schiff base with a short alkoxy substituent and a series of lanthanide(III) complexes of the type $[\text{Ln}(\text{LH})_3(\text{NO}_3)_3]$ ($\text{Ln} = \text{La}, \text{Pr}, \text{Sm}, \text{Gd}, \text{Tb}, \text{Dy}$; $\text{LH} = (E)\text{-5-(hexyloxy)-2-[(2-(2-hydroxyethylamino)ethylimino)methyl]phenol}$) have been synthesized and characterized by FTIR, ^1H and ^{13}C NMR, UV/Vis, and FAB-MS analyses. The ligand coordinates to the metal ions in its zwitterionic form. The thermal behavior of the compounds was investigated by polarizing optical

microscopy (POM) and differential scanning calorimetry (DSC). The ligand exhibits an enantiotropic hexagonal columnar (Col_h) mesophase at room temperature and the complexes show an enantiotropic lamellar columnar (Col_L) phase at around 120°C with high thermal stability. Based on XRD results, different space-filling models have been proposed for the ligand and

Keywords: density functional calculations • lanthanides • liquid crystals • luminescence • Schiff bases

complexes to account for the columnar mesomorphism. The ligand exhibits intense blue emission both in solution and in the condensed state. The most intense emissions were observed for the samarium and terbium complexes, with the samarium complex glowing with a bright-orange light (ca. 560–644 nm) and the terbium complex emitting green light (ca. 490–622 nm) upon UV irradiation. DFT calculations performed by using the DMol3 program at the BLYP/DNP level of theory revealed a nine-coordinate structure for the lanthanide complexes.

Introduction

Luminescent liquid crystals are considered immensely important materials for their potential applications in OLEDs, information storage, sensors, and enhanced contrast displays because of their excellent luminescent and charge-transporting abilities.^[1] The design and planned synthesis of liquid-crystalline molecules with specific magnetic, electronic, or luminescent properties desirable for technological applications is a challenging task for synthetic chemists. Metallocmesogens are ideal candidates for such tunable smart multi-functional properties owing to the optical, electronic, and magnetic characteristics of metal complexes with anisotropic fluids.^[2–5] Such an amalgamation of luminescent molecules and soft materials to generate new electronic devices is a fast growing field of research.^[6] The majority of metallocmesogens that have been reported up to now contain d-block metals.^[7] The design of lanthanide-containing liquid crystals is marred with complication because of their high coordination numbers that often seem to be incompatible

with the structural anisotropy required to exhibit liquid-crystalline behavior.^[8] Such materials not only possess a large magnetic anisotropy but also display interesting photophysical properties.^[9] Luminescent liquid crystals, which are useful for the design of emissive liquid crystal displays (LCDs), can be obtained by incorporating lanthanide ions into liquid crystals.^[9] In the past few years lanthanidomesogens have received considerable attention both in basic research and for their applications in the field of materials science.^[10] The first lanthanide-containing liquid crystal with a Schiff-base ligand that contained two aromatic rings was reported by Galyametdinov et al. in 1991.^[11] The complexes were shown to exhibit a highly viscous SmA mesophase. Since then a large number of lanthanidomesogens containing Schiff bases,^[8a,e–g,h,10c,e–f,12] porphyrins,^[13] phthalocyanines,^[14] β -enamino ketones,^[15] 1,2-phenanthrolines,^[16] β -diketonates,^[17] and crown ethers^[10a,18] have been investigated. A series of one-ring Schiff bases, although not mesogenic, have been complexed to lanthanides to produce ordered mesophases.^[8h,18] Very recently we reported a series of luminescent mesogenic one-ring-containing salicylaldimine Schiff bases with a long-chain substituent and their lanthanide complexes.^[19a] Both ligands and their complexes were shown to exhibit smectic mesomorphism. However, exploring the physicochemical properties of such a luminescent mesogenic compound is often hampered by their high transition temperatures. The quest for low-temperature luminescent mesogenic compounds is driven both by interest in realizing device application and academic curiosity. Since the discov-

[a] H. A. R. Pramanik, Dr. G. Das, Prof. C. R. Bhattacharjee, Dr. P. C. Paul, Dr. P. Mondal
Department of Chemistry, Assam University
Silchar 788011, Assam (India)
Fax: (+91) 03842-270342
E-mail: crbhattacharjee@rediffmail.com

[b] Dr. S. K. Prasad, Dr. D. S. S. Rao
Centre for Soft Matter Research
Jalahalli, Bangalore 560013 (India)

ery of LCDs, room-temperature liquid crystals, due to their high thermal stability, have enjoyed significant attention.^[12g] Set in this backdrop, in this article we report the synthesis of a new one-ring O-donor Schiff base derived from an amino alcohol and its lanthanide complexes $[\text{Ln}(\text{LH})_3(\text{NO}_3)_3]$ ($\text{Ln}=\text{La, Pr, Sm, Gd, Tb}$), which are both liquid crystalline and luminescent, exhibiting hexagonal columnar mesomorphism. Interestingly, the ligand is mesogenic at room temperature. Although a luminescent liquid crystalline one-ring Schiff base has recently been recorded,^[19a] this appears to be the first example of a room-temperature-based one-ring Schiff-base mesogen. Also pertinent here is to mention that there is no report of a one-ring lanthanidomesogen that exhibits columnar mesomorphism.

Results and Discussion

Synthesis and structural assessment: The Schiff-base ligand LH ((E)-5-(hexyloxy)-2-{[2-(2-hydroxyethylamino)ethylimino]methyl}phenol, abbreviated as **6ae**) was obtained from the condensation of a 4-alkoxy-substituted aldehyde with a 2-(2-aminoethylamino)ethanol by a slight modification of the literature procedure.^[19a] The complexes (Ln-6ae) were prepared by the reaction of the ligand with the appropriate metal nitrate in a 1:3 ratio of Ln/LH in ethanol/acetonitrile at ambient temperature and obtained as cream-colored solids in good yields. The elemental analyses revealed the stoichiometry of the complexes to be consistent with the formula $[\text{Ln}(\text{LH})_3(\text{NO}_3)_3]$ (Scheme 1). The ν_{CN} peak at around 1625 cm^{-1} observed for the ligand undergoes a hypsochromic shift to around 1656 cm^{-1} in all the complexes on account of zwitterion formation. Moreover, the appearance of a weak broad band at about 3047 cm^{-1} reflects the zwitterionic (-C=N⁺H) nature of the ligand. The coordinating ni-

trate groups appear at characteristic frequencies of around $1484 (\nu_1)$, $1300 (\nu_4)$, $1141 (\nu_2)$, and $813 \text{ cm}^{-1} (\nu_3)$, and the difference between the two strongest absorptions (ν_1 and ν_4) of the nitrate groups is about 180 cm^{-1} , which clearly shows that the NO_3^- groups in the solid complexes coordinate to the lanthanide ion as bidentate ligands.^[8f, 10c, 20] The FAB mass spectra of the ligand and their Ln^{III} complexes are in good agreement with their formula masses. The ¹H NMR spectrum of the diamagnetic lanthanum(III) complex shows that the signal corresponding to the imine hydrogen, $\text{CH}=\text{N}$, is split into a doublet ($\delta=7.61$ and 7.62 ppm with ${}^3J_{\text{H-H}}=12 \text{ Hz}$) in contrast to the singlet of the free Schiff-base ligand ($\delta=8.11 \text{ ppm}$), which suggests protonation of the imine nitrogen. Furthermore, a new signal, characteristic of an $\text{N}^+ \text{H}$ resonance, appears in the spectrum of the complex at $\delta=12.07 \text{ ppm}$, precluding any coordination involving the imine nitrogen. These observations are in good agreement with systems reported previously.^[8f, 10c, 19a, 20]

Photophysical properties: The electronic spectra (Figure 1) of the compounds were recorded in chloroform solution. The ligand shows three bands in the region 285 – 390 nm . The bands centered at around 285 and 309 nm are due to the $\pi-\pi^*$ transition localized on the aromatic ring and that at

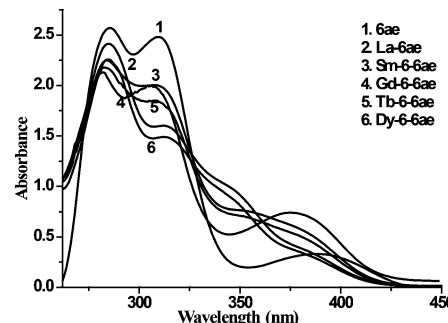
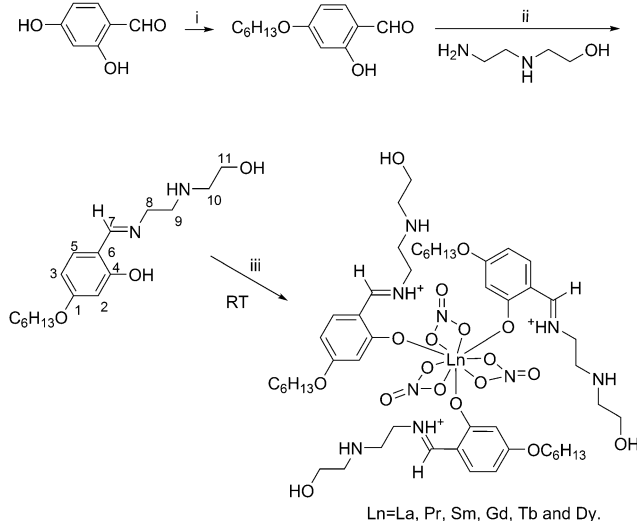


Figure 1. UV/Vis spectra of **6ae** and Ln-6ae in CH_2Cl_2 (10^{-4} M solution).



Scheme 1. Reagents and conditions: i) $\text{C}_6\text{H}_{13}\text{Br}$, KHCO_3 , KI , dry acetone, Δ , 40 h ; ii) glacial AcOH , absolute EtOH , Δ , 4 h ; iii) $\text{Ln}(\text{NO}_3)_3 \cdot 6 \text{ H}_2\text{O}$, acetonitrile, stirring, RT, 3 h .

around 390 nm is due to the $\pi-\pi^*$ transition of the imine chromophore. Upon complexation, these bands are blue-shifted to around 284 , 307 – 313 , and 347 – 376 nm . A photoluminescence study of the ligand (Figure 2) and its complexes was carried out in the solid, solution, and mesomorphic states. As the ligand is mesogenic at room temperature, the luminescent spectra were recorded in both the solid state and in solution. In solution, the ligand shows one emission maximum at around 436 nm in solution, however, in the solid state (mesomorphic), the emission maximum is redshifted to around 446 nm . In the condensed state, the larger intermolecular interaction gives rise to greater electronic delocalization resulting in a lowering in the energy of the electronic states and hence the emission maximum is redshifted. In general, Schiff-base systems exhibit fluorescence due to intraligand $\pi-\pi^*$ transitions.^[21] Surprisingly, the complexes all exhibit similar emission maxima in the solution, solid, and mesomorphic states. The emission maxima

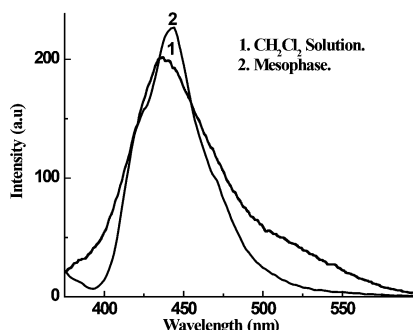


Figure 2. Photoluminescence spectra of **6ae** ($\lambda_{\text{exc}} = 350 \text{ nm}$) in solution and in the solid state (mesophase).

can be tuned by changing the metal ions. The samarium(III) complex, $[\text{Sm}(\text{LH})_3(\text{NO}_3)_3]$, glows with a bright-orange light both in the solid and solution states upon UV irradiation (Figure 3). The emission spectrum exhibits three characteristic transitions originating from the Sm^{3+} lowest emitting

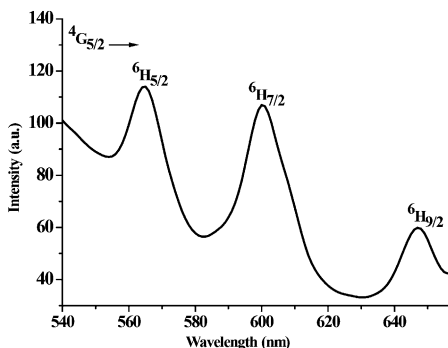


Figure 3. Photoluminescence spectrum of Sm-6ae in the solid state ($\lambda_{\text{exc}} = 350 \text{ nm}$).

state $^4\text{G}_{5/2}$ to the $^6\text{H}_{9/2}$ (644 nm, $\Phi = 18\%$), $^6\text{H}_{7/2}$ (603 nm), and $^6\text{H}_{5/2}$ (565 nm) levels.^[22,23] The ligand is excited to its singlet state and through intersystem crossing transit to their triplet state. The energies of the singlet and triplet states are then intramolecularly transferred to the energy level of the Sm^{3+} ion. Luminescence is observed during radiative deactivation to the ground state. The Tb^{3+} complex, an intense green emitter, shows characteristic emission bands ($\lambda_{\text{ex}} = 350 \text{ nm}$) centered at around 491, 548, 583, and 621 nm, resulting from the deactivation of the $^5\text{D}_4$ excited state to the corresponding ground state $^7\text{F}_J$ ($J = 6, 5, 4, 3$) of the Tb^{3+} ion (Figure 4). The most intense narrow emission band centered at around 548 nm ($\Phi = 16\%$) corresponds to the hypersensitive metal-based transition $^5\text{D}_4 \rightarrow ^7\text{F}_5$.^[19b] The lanthanum ($3\text{d}^{10}4\text{f}^0$) complex in solution exhibits a rather broad and strong green emission at around 542 nm caused by ligand-to-metal charge transfer (LMCT) excited states not observed for the other lanthanide complexes ($3\text{d}^{10}4\text{f}^n$); the praseodymium, gadolinium, and dysprosium complexes show strong blue-light emission with maxima at around 420–

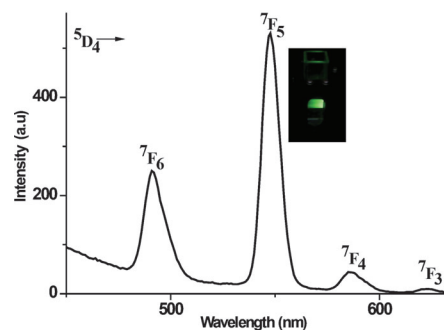


Figure 4. Photoluminescence spectrum of Tb-6ae in the solid state ($\lambda_{\text{exc}} = 350 \text{ nm}$). Inset shows fluorescent image of Tb-6ae.

435 nm (Figure 5) upon photoexcitation at around 350 nm. These emissions occur from a predominantly ligand-based $^1\pi\pi^*$ excited state.^[22d] The observed photoluminescence behavior closely resembles similar systems reported recently.^[19a–c]

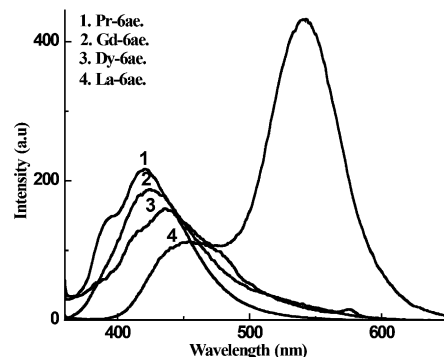


Figure 5. Photoluminescence spectra of La/Pr/Gd/Dy-6ae in solution ($\lambda_{\text{exc}} = 350 \text{ nm}$).

Thermal properties and liquid-crystalline behavior: The thermal properties of the ligand and its complexes were studied by using polarizing optical microscopy (POM) and differential scanning calorimetry (DSC). The ligand was found to exhibit enantiotropic mesomorphism at room temperature. The sample placed between two glass slides can be easily sheared to show birefringent textures, which clearly indicates that the compound is already in the liquid-crystalline state at room temperature. No melting/crystallization peak was observed in the DSC thermogram (Table 1); the ligand transforms directly into an isotropic liquid at 35°C. Upon cooling, first batonnets appear from the isotropic melt, which coalesce to a fan-like texture (Figure 6) with several homeotropic regions at 28°C. The mesophase was identified as a hexagonal columnar (Col_h) phase through an XRD study (see above). The ligand with a short C_6 alkoxy terminal chain is not a simple calamitic species, the presence of the alcoholic OH group tends to induce attractive intermolecular interactions involving HO···HO hydrogen bonds, resulting in liquid-crystalline behavior. The DSC thermo-

Table 1. DSC data for **6ae** and its complexes.^[a]

Compounds	Heating	Cooling
6ae	Col _h 35.5 (6.1) I	I 28 (5.2) Col _h
La- 6ae	Cr 75.8 (34.9) Col _L 120.9 (4.6) I	I 119.2 (4.6) Col _L 45.6 (20.2) Cr
Pr- 6ae	Cr 76.7 (35.6) Col _L 121.3 (4.5) I	I 120.8 (4.4) Col _L 44.9 (20.1) Cr
Sm- 6ae	Cr 67.3 (33.2) Col _L 118.8 (4.7) I	I 117.5 (4.5) Col _L 43.6 (21.4) Cr
Gd- 6ae	Cr 69.8 (35.6) Col _L 116.7 (4.9) I	I 115.8 (4.7) Col _L 41.2 (24.3) Cr
Tb- 6ae	Cr 73.7 (28.7) Col _L 113.9 (3.8) I	I 111.7 (3.5) Col _L 38.7 (18.7) Cr
Dy- 6ae	Cr 63.5 (24.3) Col _L 117.9 (4.1) I	I 116.3 (3.5) Col _L 35.6 (17.1) Cr

[a] Temperatures in °C.



Figure 6. POM texture of **6ae**.

4.6 kJ mol⁻¹) is due to the I→Col_L phase transition. A similar observation was also noted for all the other complexes (Table 1). The mesophase to the clearing point transition temperature decreases along the lanthanide series, which is in accord with a recent observation on related lanthanide complexes.^[9a,19a] The reversibility of the thermal behavior was established by DSC in subsequent heating/cooling cycles. One-ring Schiff-base complexes of lanthanides, irrespective of their stoichiometric

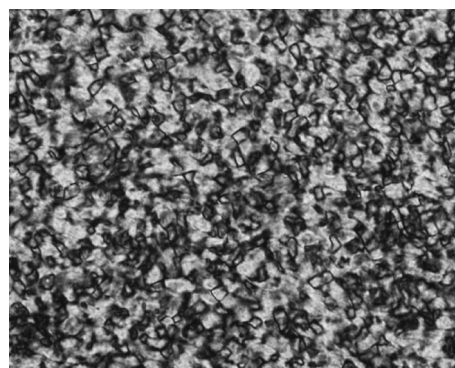


Figure 7. POM texture of Sm-**6ae**.

gram of **6ae** shows a broad peak at around 35°C in the heating process and a peak at around 28°C in the cooling process. As the mesophase appears in both the heating and cooling cycles the mesophase is enantiotropic. The peak at 28°C ($\Delta H=5.2\text{ kJ mol}^{-1}$) is due to an I→Col_h phase transition. Note that the mesophase-to-isotropic transition temperature is higher for analogous Schiff-base compounds studied in our earlier work than that observed in the present case.^[19a] This is quite unusual considering the fact that the pendant alkoxy chain in **6ae** contains only six carbon atoms compared with the 18 carbon atoms in the alkoxy chain in the previously reported compounds.^[19a] The effect of a lateral substituent on the melting point and the isotropic–mesomorphic transition temperature may also be significant. The replacement of the OH group of the aminoethanol part by the -NHCH₂CH₂OH fragment in this case increases the width of the molecule and presumably the intermolecular distance, which may have led to a reduction in the lateral intermolecular attractive force and consequent drastic depression of the melting and clearing points.

The complexes exhibit enantiotropic mesomorphism and a viscous waxy appearance before melting to an isotropic liquid. Upon cooling, the complexes also show mosaic textures (Figure 7) reminiscent of a lamellar columnar (Col_L) mesophase, which tend to decompose on further heating after reaching the isotropic temperature. By pressing with a needle on the microscopic cover glass, it is possible to observe birefringence, although the molecules quickly reorient to the homeotropic alignment. The DSC trace of a typical complex, Sm-**6ae**, displays two transitions in both the heating and cooling cycles (Figure 8). The transitions are very sharp and well defined. The peak at 117.5°C ($\Delta H=$

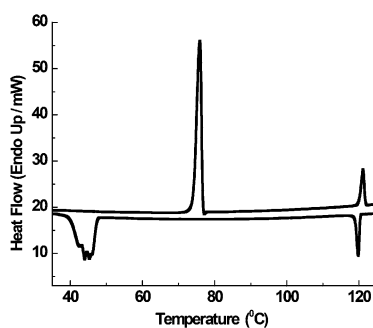


Figure 8. DSC thermogram of Sm-**6ae**.

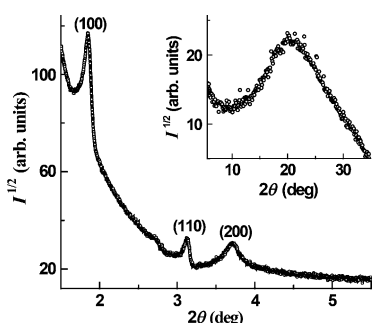
type, invariably exhibit smectic mesomorphism.^[8h] In this regard, the present complexes are the first of their kind that exhibit columnar mesomorphism.

X-ray diffraction study of the ligand (6ae**) and its samarium complex (Sm-**6ae**):** Temperature-dependent, small-angle X-ray diffraction experiments were carried out to identify unequivocally the nature of the mesophase. The diffraction pattern (Table 2) for the ligand **6ae** was obtained at 28°C in the mesophase (Figure 9). In the wide-angle region, a diffuse intensity maximum centered at around 4.2 Å is observed. This is associated with the short-range liquid-like positional ordering of the hydrocarbon chains within the layer plane. In the low-angle region, sharp peaks observed corresponding to *d* spacings of 47.7, 28.2, and 23.8 Å in the ratio 1:0.59:0.5 suggest a columnar phase with 2D hexagonal ordering with a lattice dimension of 56.1 Å.^[24a] Pertinent here

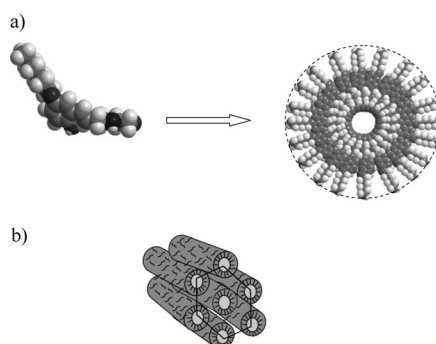
Table 2. PXRD data for **6ae** and Sm-**6ae**.

Compound	Mesophase parameters ^[a]	d_{obsd} [Å] (d_{calcd} [Å]) ^[b]	Miller indices ^[c]
6ae	Col _h , 28°C $a=56.11$ Å $S=2725.5$ Å ² $V_m=511.8$ Å ³ $h=4.2$	47.71 (47.73) 28.23 (28.24) 23.81 (23.83) 4.2	(100) (110) (200)
$N=21$			
Sm- 6ae	Col _L , 110°C $d=37.61$ Å $V_m=2025$ Å ³	37.50 (37.61) 18.76 (18.80) 12.93 (12.54) 11.25 (11.26) 8.6 (h) 7.71 (7.70) 4.3 (h _{ch})	(100) (200) (300) (120) (130)

[a] For the Col_h mesophase, the lattice parameters are deduced from the following mathematical expressions for the columnar phase: $\langle d_{100} \rangle = 1/N_{hk}[\sum d_{hk}(h^2+k^2+hk)^{1/2}]$, in which N_{hk} is the number of hk reflections, and $a=2\langle d_{100} \rangle / \sqrt{3}$. The molecular volume, V_m , is calculated by using the formula $V_m=M/\lambda\rho N_A$, in which M is the molecular weight of the compound, N_A is Avogadro's number, ρ is the volume mass (≈ 1 g cm⁻³), $\lambda(T)$ is a temperature correction coefficient at the temperature of the experiment (T). The intracolumnar repeating distance h is calculated directly from the estimated molecular volume V_m according to the equation $h=NV_m/S$, in which N is the number of molecules and S is the lattice area (columnar cross-section). For a hexagonal lattice $S=a^2\sqrt{3}/2$. For the Col_L phase, $d=\sum d_{100}/N_{100}$, in which N_{100} is the number of 100 reflections. [b] d_{obsd} and d_{calcd} are the experimentally measured and theoretical diffraction spacings, respectively. [c] Miller indices (hkl) of the reflections of the Col_h and Col_L phases.

Figure 9. XRD profile of **6ae**.

is to mention that in addition to planar disc-like molecules, many other molecular shapes may also give rise to a columnar-type of organization.^[24b-h] The lattice constant ($a=56.1$ Å) is much larger than the monomeric molecular length of 28.04 Å for a fully extended molecule, as calculated from a DFT study. The following model (Figure 10) could be deduced for the organization of the tapered molecules of the ligand **6ae** with nonequivalent ends in the columnar mesophase. The aliphatic tails diverge towards the periphery of the column, whereas the polar and hydrogen-bonding moieties (OH groups) of the molecule reside near the center, surrounded by an aromatic crown. The construction of the disc resulting from the stacking of 21 tapered units of **6ae** side

Figure 10. Molecular organization in the mesophase of **6ae**. a) Cross-section through a single column constructed by the self-assembly of the tapered shape molecules. b) Arrangement of the columns in a hexagonal lattice.

by side in a radial conformation is presented in Figure 10. This leads to tubular columns,^[24b-f] generated by the stacking of the discs, and the mutual organization of these columns into a hexagonal lattice leads to the formation of the mesophase. This further explains the observed variation in the peak intensity in Figure 9, reflecting a hole in the electronic density distribution. The effective diameter of the columns is assumed to match the experimentally observed lattice constant ($a=56.1$ Å). In this arrangement, the terminal aliphatic chains are rather disorganized, which confine the rigid cores by forming a liquid matrix-like structure around them. Considering a density close to 1 g cm⁻³ and a periodic stacking of the molecular cores within a column of 4.2 Å, there are approximately 21 molecules per unit cell ($N=hS/V_m$). In a hexagonal lattice, there is one column per unit cell. The large number of molecules ($N=21$) in the cross-section of the columns is probably due to the small taper angle with a minimum space requirement of the peripheral alkoxy chains, whereas the hydrogen-bonding fragment is tightly packed in the middle of the column cores. Although such a large number of molecules per column is quite uncommon, it is not unprecedented.^[24g] The observed stacking distance within a column ($h=4.2$ Å) is greater than that expected (3.5 Å) for π-π stacking with a “face-to-face” orientation of the aromatic cores. This is accounted for by invoking “edge-to-edge” stacking of the molecules in the column.^[24h] Therefore that the tapered rod-like molecular motifs may also lead to the supramolecular columnar liquid-crystalline assembly.

For the complex Sm-**6ae**, three peaks (Figure 11) were observed in the small-angle region, one strong peak and two weak peaks corresponding to the Miller indices (100), (200), and (300) with a d -spacing ratio of 1:2:3, respectively.^[25a] The presence of these equidistant reflections shows that the molecules are arranged in regularly spaced layers (Figure 12) with a layer distance of 37.61 Å. Two other less intense but relatively sharp reflections were assigned to (120) and (130) reflections, which indicate 2D columnar ordering of the mesophase. The presence of broad halos in the wide-angle region at 4.3 (h_{ch}) and 8.6 Å confirm the fluid

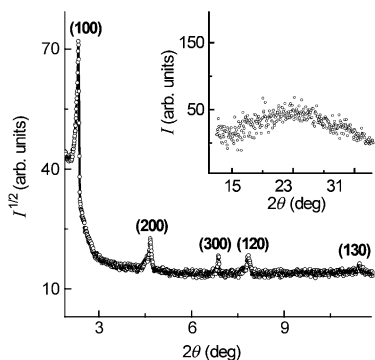
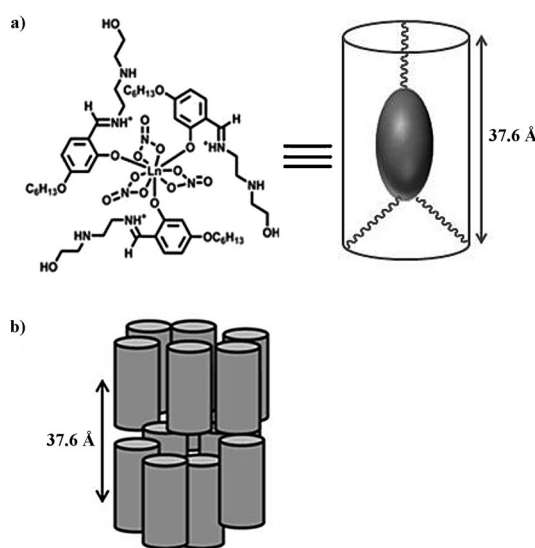


Figure 11. XRD profile of Sm-6ae.

nature of the mesophase; the former corresponds to the molten chains in liquid-like order, whereas the latter is ascribed to double periodicity. The peak centered at 20.85° (4.3 \AA) is much wider, extending to around $2\theta=35^\circ$, than that expected for an archetypical disordered mesophase.

Figure 12. a) Lanthanide complex containing three Schiff-base ligands bearing a C_6 alkoxy chain. b) Organization of molecules in the Col_L phase.

The XRD analysis therefore reveals that the observed mesophase may more appropriately be branded as a lamellar phase with short-range columnar order within the layers (Col_L).^[25b,c] As such, the phase is more akin to a smectic-type phase. The cross-sectional area ($A=2V_M/d$) deduced from the molecular volume ($V_M=2025\text{ \AA}^3$) and the layer thickness ($d=37.61\text{ \AA}$) is around 108 \AA^2 . Considering a total of three alkoxy chains, a cross-sectional area of 36 \AA^2 ($A/3$) per mesogenic unit is obtained. The Col_L mesophase can be imagined to form smectic layers made of broken lamellae with some interdigitation of the peripheral alkoxy chains in the layer molecules (Figure 12).

DFT study of Gd-6ae: As single crystals suitable for X-ray analysis could not be grown, DFT studies were undertaken to ascertain the optimized geometry of the Gd-6ae complex. The ground-state geometries of the Gd-6ae complex in the gas phase were fully optimized by using the unrestricted BLYP/DNP methods without imposing any symmetry constraints. The BLYP functional, used throughout this study, comprises a hybrid exchange functional as defined by Becke and the nonlocal Lee-Yang-Parr correlation functional.^[26c] The basis set chosen was DNP, double-numerical atomic orbitals augmented by polarization functions.^[26a-d] Relativistic effects were taken into account by using an all-electron scalar relativistic method based on the Douglas-Kroll-Hess (DKH) transformation.^[26a-d] All calculations were performed with the DMol3 program package^[26d]. All three nitrophenolate groups coordinate to the gadolinium ion in a bidentate fashion. With the phenolic proton transferred to the imine nitrogen, the phenolate oxygen binds the gadolinium ion in a monodentate fashion (Figure 13). With three monodentate

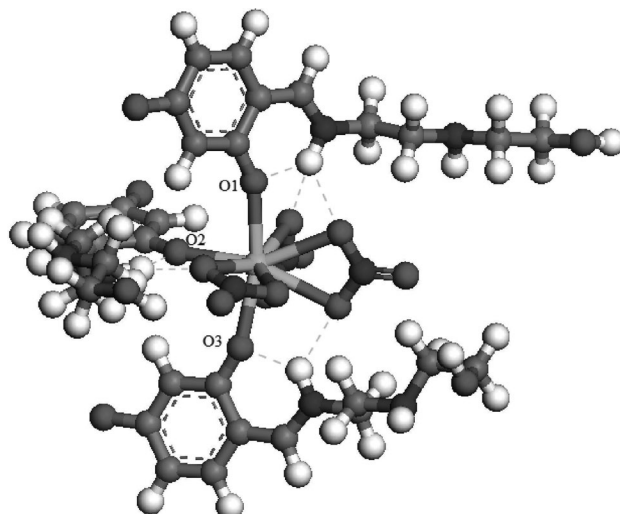


Figure 13. Optimized structure of Gd-6ae.

O-donor Schiff-base ligands and as many chelated bidentate nitrophenolate groups, the gadolinium ion achieves a nine-coordinate geometry quite typical of lanthanides. Two of the three imine protons form double hydrogen bonds with the phenolate oxygen and with an oxygen atom of a nitrophenolate group, whereas the third proton forms two hydrogen bonds with two nitrophenolate oxygen atoms and one with a phenolic oxygen atom of a ligand. The HOMO and LUMO energies of the complex Gd-6ae were calculated to be -4.947 and -2.668 eV , respectively ($\Delta E=2.279\text{ eV}$). The HOMO-LUMO energy gap is a measure of the kinetic stability of a molecule and could indicate its reactivity pattern. A large HOMO-LUMO gap implies high kinetic stability and low chemical reactivity because it is energetically unfavorable to add electrons to a high-lying LUMO or to extract electrons from a low-lying HOMO. The high HOMO-LUMO energy

gap of 2.279 eV in the present case suggests the complex to be quite stable. The calculated average Gd–O (nitroato) and Gd–O (phenolic) bond distances in the Gd–**6ae** complex are 2.578 and 2.410 Å, respectively, and the bond angles O1–Gd–O2, O2–Gd–O3, and O1–Gd–O3 are 88.3, 83.2, and 160.5°, respectively. Mutually perpendicular to each other, the phenyl rings of the three Schiff-base ligands with the short hexyloxy tail are located as far as possible from each other in the three-dimensional space.

Conclusion

A new series of emissive lanthanidomesogens, $[\text{Ln}(\text{LH})_3(\text{NO}_3)_3]$ ($\text{Ln}=\text{La, Pr, Sm, Gd, Tb, Dy}$; $\text{LH}=(E)\text{-5-(hexyloxy)-2-[2-(2-hydroxyethylamino)ethylimino]methylphenol}$) have been successfully synthesized. The ligand and complexes are both liquid crystalline and photoluminescent. The ligand with a short C₆ alkoxy tail showed hexagonal columnar mesomorphism at room temperature. The complexes were found to be thermally very stable. The Schiff-base ligand exists as a zwitterion in the complexes, binding to the metal in a monodentate fashion through the phenolate oxygen and the nitroato groups chelating to the metal to complete the nine coordination around the lanthanide ion. Although one-ring Schiff-base complexes of lanthanides, regardless of their stoichiometries, are known to exhibit smectic mesomorphism,^[19a] the newly reported complexes exhibiting lamello-columnar mesomorphism are the first of their kind. The samarium(III) complex shows ligand-sensitized bright-orange emission on excitation at 350 nm with a high quantum yield of around 18%, whereas the other complexes are blue or green emitters. The complexes are anticipated to serve as promising candidates for multifunctional device applications.

Experimental Section

Physical measurements: The C, H, and N analyses were carried out on a PE2400 elemental analyzer. NMR spectra were recorded on a Bruker DPX 400 MHz spectrometer in CDCl₃ (chemical shifts in ppm) with TMS as internal standard. The UV/Vis absorption spectra of the compounds in CHCl₃ were recorded on a Shimadzu UV-160PC spectrophotometer. IR spectra were recorded on a Perkin-Elmer L 120-000A spectrometer in KBr discs. The mass spectra were recorded on a JEOL SX-102 FAB mass spectrometer. Magnetic susceptibility measurements were made at room temperature on a Cahn-Faraday balance. The optical textures of the different phases of the compounds were studied by using a polarizing microscope (Nikon optiphot-2-pol) attached to an Instec hot and cold stage HCS302 microscope with an STC200 temperature controller with an accuracy of 0.1°C. The thermal behavior of the compounds was studied by using a Perkin-Elmer Pyris-1 differential scanning calorimeter (DSC) at heating and cooling rates of 5°C min⁻¹. X-ray measurements were carried out by using samples filled in Lindemann capillaries. The apparatus essentially involved a PANalytical X'Pert PRO MP X-ray diffractometer consisting of a focussing elliptical mirror and a fast high-resolution detector. The wavelength of the radiation employed is 0.15418 nm. Photoluminescence spectra were recorded on a Shimadzu RF-53D1 PC instrument. The fluorescence quantum yields were deter-

mined by using quinine bisulfate in 0.1 N H₂SO₄) as standard. Quantum chemical calculations were carried out on **6ae** and Gd–**6ae** by using density functional theory (DFT) as implemented in the DMol3 package.^[26d]

Materials: All solvents were purified and dried following standard procedures. The materials were procured from Tokyo Kasei and Lancaster Chemicals. Silica (60–120 mesh) from Spectrochem was used for chromatographic separation. Silica gel G (E-Merck, India) was used for TLC.

Synthesis and analysis

4-(Hexyloxy)salicylaldehyde: 4-Alkoxysalicylaldehyde derivatives were prepared following the general method reported in the literature.^[3] 2,4-Dihydroxybenzaldehyde (10 cm³, 1.38 g), KHCO₃ (10 cm³, 1 g), KI (catalytic amount), and 1-bromohexane (10 mmol, 1.6 g) were mixed in dry acetone (250 cm³). The mixture was heated under reflux for 40 h and then filtered, while hot, to remove any insoluble solids. Dilute HCl was added to neutralize the warm solution, which was then extracted with chloroform (100 cm³). The combined chloroform extract was concentrated to give a purple solid, which was purified by column chromatography using a mixture of chloroform and hexane (1:1, v/v) as eluent. Evaporation of the solvents afforded a white solid product.

(E)-5-(Hexyloxy)-2-[2-(2-hydroxyethylamino)ethylimino]methylphenol (6ae): An ethanolic solution of 2-hydroxy-4-(hexyloxy)salicylaldehyde (0.22 g, 1 mmol) was added to an ethanolic solution of 2-(2-aminoethylamino)ethanol (0.10 g, 1 mmol). The mixture was heated at reflux with a few drops of acetic acid as catalyst for 3 h to yield the yellow Schiff base. The compound was collected by filtration and recrystallized from absolute ethanol to obtain a pure compound. Yield: 0.245 g, 75%; yellow solid; ¹H NMR (400 MHz, CDCl₃): δ = 1.3 (t, J = 8 Hz, 3H; CH₃), 1.46–1.74 (m, CH₂ of in side-chain), 3.61 (t, J = 4.0 Hz, 2H; CH₂N=C), 3.70 (t, J = 4.0 Hz, 2H; CH₂OH), 3.84 (t, J = 8 Hz, 2H; OCH₂), 7.09 (d, J = 8.3 Hz, 1H; C₆H₄), 8.11 (s, 1H; N=CH), 13.14 ppm (s, 1H, OH); ¹³C NMR (75.45 MHz, CDCl₃, Me₄Si at 25°C): δ = 161.3 (C-1), 102.3 (C-2), 107.4 (C-3), 161.6 (C-4), 131.3 (C-5), 116.7 (C-6), 160.8 (C-7), 55.4 (C-8), 68.4 (OCH₂), 50.5 (C-9), 52.0 (C-10), 61.5 (C-11) ppm; IR (KBr): ν = 3457 (vOH), 2924 (v_{as}C–H, CH₃), 2922 (v_{as}C–H, CH₂), 2871 (v_sC–H, CH₃), 2849 (v_{as}C–H, CH₂), 1625 (vC=N), 1297 cm⁻¹ (vC–O); MS (FAB): m/z: calcd for C₁₇H₂₈N₂O₃ 308.2; found: 309 [M+H]⁺; elemental analysis calcd (%) for C₁₇H₂₈N₂O₃ (308.2): C 66.2, H 9.1, N 9.0; found: C 66.1, H 9.2, N 9.1.

Synthesis of the lanthanide(III) complexes $[\text{Ln}(\text{LH})_3(\text{NO}_3)_3]$ ($\text{LH}=\text{6ae}$): A solution of $\text{Ln}(\text{NO}_3)_3\cdot 6\text{H}_2\text{O}$ [$\text{Ln}=\text{La}$ (1 mmol, 0.43 g), Pr (1 mmol, 0.43 g), Sm (1 mmol, 0.44 g), Gd (1 mmol, 0.51 g), Tb (1 mmol, 0.43 g), Dy (1 mmol, 0.45 g)] in a minimum volume of acetonitrile was added dropwise to an ethanolic solution of ligand **6ae** (3 mmol, 0.92 g) at room temperature. The reaction mixture was stirred for 3 h and the cream-colored solid that formed was filtered and washed with absolute ethanol and dried in vacuo.

[La(LH)₃(NO₃)₃] (La–6ae): Yield: 1 g, (78%); cream-colored solid; ¹H NMR (400 MHz, CDCl₃): δ = 1.3 (t, J = 6.9 Hz, 9H; 3 CH₃), 1.45–1.78 (m, 3 CH₂ of side-chain), 6.64 (d, J = 8.8 Hz, 3H; 3 C₆H₄), 7.61 (d, J = 12 Hz, 3H; 3 CH=N), 12.31 (br, s, 3 N⁺H), 3.70 ppm (t, J = 4.0 Hz, 6H; 3 CH₂OH); IR (KBr): ν = 3317 (vOH, CH₂OH), 1241 (vC–O, ether), 1655 (vC=N), 1475 (v₄NO₃), 1290 (v₁NO₃), 1135 (v₂NO₃), 855 cm⁻¹ (v₆NO₃); MS (FAB): m/z calcd for LaC₄₈H₇₈N₉O₁₈ 1207.4; found: 1208 [M+H]⁺; elemental analysis calcd (%) for LaC₄₈H₇₈N₉O₁₈ (1207.4): C 47.7, H 6.5, N 10.4; found: C 47.7, H 6.4, N 10.5.

[Pr(LH)₃(NO₃)₃] (Pr–6ae): Yield: 1.18 g, (76%); cream-colored solid; IR (KBr): ν = 3314 (vOH, CH₂OH), 1240 (vC–O, ether), 1658 (vC=N), 1474 (v₄NO₃), 1289 (v₁NO₃), 1132 (v₂NO₃), 850 cm⁻¹ (v₆NO₃); MS (FAB): m/z: calcd for PrC₄₈H₇₈N₉O₁₈ 1209.4; found: 1210 [M+H]⁺; elemental analysis calcd (%) for PrC₄₈H₇₈N₉O₁₈ (1209.4): C 47.6, H 6.5, N 10.4; found: C 47.5, H 6.6, N 10.4.

[Sm(LH)₃(NO₃)₃] (Sm–6ae): Yield: 1 g, (76%); cream-colored solid; IR (KBr): ν = 3310 (vOH, CH₂OH), 1235 (vC–O, ether), 1659 (vC=N), 1473 (v₄NO₃), 1288 (v₁NO₃), 1133 (v₂NO₃), 851 cm⁻¹ (v₆NO₃); MS (FAB): m/z: calcd for SmC₄₈H₇₈N₉O₁₈ 1220.4; found: 1221 [M+H]⁺; elemental analysis calcd (%) for SmC₄₈H₇₈N₉O₁₈ (1220.4): C 47.2, H 6.4, N 10.3; found: C 47.1, H 6.4, N 10.2.

[Gd(LH)₃(NO₃)₃] (Gd-6ae): Yield: 1.1 g, (78%); cream-colored solid; IR (KBr): $\tilde{\nu}$ =3314 (vOH, CH₂OH), 1241 (vC—O, ether), 1651 (vC=N), 1471 (v₄NO₃), 1281 (v₁NO₃), 1129 (v₂NO₃), 853 cm⁻¹ (v₆NO₃); MS (FAB): *m/z*: calcd for GdC₄₈H₇₈N₉O₁₈ 1226.4; found: 1227 [M+H]⁺; elemental analysis calcd (%) for GdC₄₈H₇₈N₉O₁₈ (1226.4): C 47.0, H 6.4, N 10.2; found: C 47.1, H 6.3, N 10.2.

[Tb(LH)₃(NO₃)₃] (Tb-6ae): Yield: 1.0 g, (76%); cream-colored solid; IR (KBr): $\tilde{\nu}$ =3319 (vOH, CH₂OH), 1245 (vC—O, ether), 1653 (vC=N), 1473 (v₄NO₃), 1283 (v₁NO₃), 1127 (v₂NO₃), 851 cm⁻¹ (v₆NO₃); MS (FAB): *m/z*: calcd for TbC₅₇H₁₀₅N₉O₁₈ 1363.6; found: 1364 [M+H]⁺; elemental analysis calcd (%) for TbC₅₇H₁₀₅N₉O₁₈ (1363.6): C 50.2, H 7.7, N 9.2; found: C 50.1, H 7.5, N 9.3.

[Dy(LH)₃(NO₃)₃] (Dy-6ae): Yield: 1.0 g, (75%); cream-colored solid; IR (KBr): $\tilde{\nu}$ =3321 (vOH, CH₂OH), 1248 (vC—O, ether), 1658 (vC=N), 1475 (v₄NO₃), 1282 (v₁NO₃), 1125 (v₂NO₃), 856 cm⁻¹ (v₆NO₃); MS (FAB): *m/z*: calcd for DyC₅₇H₁₀₅N₉O₁₈ 1367.6; found: 1368 [M+H]⁺; elemental analysis calcd (%) for DyC₅₇H₁₀₅N₉O₁₈ (1367.6): C 50.0, H 7.7, N 9.2; found: C 50.2, H 7.5, N 9.2%.

Acknowledgements

The authors thank the Sophisticated Analytical Instrument Facility, North-Eastern Hill University (SAIF, NEHU) and the Central Drug Research Institute (CDRI) for analytical and spectral data. H.A.R.P. is thankful to the Council of Scientific and Industrial Research (New Delhi) for a research fellowship (No. 09/747(0006)/2011-EMR-I).

- [1] a) R. J. Bushby, O. R. Lozman, *Curr. Opin. Colloid Interface Sci.* **2002**, *7*, 343–354; b) M. O'Neill, S. M. Kelly, *Adv. Mater.* **2003**, *15*, 1135–1146; c) J. Hanna, *Opto-Electron. Rev.* **2005**, *13*, 259–267.
- [2] a) R. Bayón, S. Coco, P. Espinet, *Chem. Eur. J.* **2005**, *11*, 1079–1085; b) V. N. Kozhevnikov, B. Donnio, D. W. Bruce, *Angew. Chem.* **2008**, *120*, 6382–6385; *Angew. Chem. Int. Ed.* **2008**, *47*, 6286–6289; c) A. Santoro, A. C. Whitwood, J. A. G. Williams, V. N. Kozhevnikov, D. W. Bruce, *Chem. Mater.* **2009**, *21*, 3871–3882.
- [3] C. Weder, C. Sarwa, C. Bastiaansen, P. Smith, *Adv. Mater.* **1997**, *9*, 1035–1039.
- [4] Y. G. Galyametdinov, A. A. Knyazev, V. I. Dzhabarov, T. Cardinaels, K. Driesen, C. Gorller-Walrand, K. Binnemans, *Adv. Mater.* **2008**, *20*, 252–257.
- [5] D. W. Bruce, R. Deschenaux, B. Donnio, D. Guillon in *Comprehensive Organometallic Chemistry III, Volume 12* (Eds.: D. M. P. Mingos, R. H. Crabtree, D. O'Hare), Elsevier, Oxford, **2007**, 195.
- [6] a) K. Binnemans, *J. Mater. Chem.* **2009**, *19*, 448–453; b) Y. Wang, Y. Liu, H. Qi, X. Li, M. Nin, M. Liu, D. Shi, W. Zhu, Y. Cao, *Dalton Trans.* **2011**, *40*, 5046–5051.
- [7] a) A. M. Giroud-Godquin, P. M. Maitlis, *Angew. Chem.* **1991**, *103*, 370–398; *Angew. Chem. Int. Ed. Engl.* **1991**, *30*, 375–402; b) P. Espinet, M. A. Esteruelas, L. A. Oro, J. L. Serrano, E. Sola, *Coord. Chem. Rev.* **1992**, *117*, 215–274; c) S. A. Hudson, P. M. Maitlis, *Chem. Rev.* **1993**, *93*, 861–885; d) D. W. Bruce, *J. Chem. Soc. Dalton Trans.* **1993**, 2983–2989; e) A. P. Polishchuk, T. V. Timofeeva, *Russian Chem. Rev.* **1993**, *62*, 291–321; f) J. L. Serrano, *Metalomesogens, Synthesis Properties and Applications*, Wiley-VCH, Weinheim, **1996**; g) A. M. Giroud-Godquin, *Coord. Chem. Rev.* **1998**, *178–180*, 1485–1499; h) B. Donnio, D. W. Bruce, *Struct. Bonding (Berlin)* **1999**, *95*, 193–247.
- [8] a) Yu. G. Galyametdinov, G. I. Ivanova, A. V. Prosvirin, O. Kadkin, *Russ. Chem. Bull.* **1994**, *43*, 938–940; b) Y. G. Galyametdinov, M. A. Athanassopoulou, K. Griesar, O. Kharitonova, E. A. Soto, W. Bustamante, L. Tinchurina, I. Ovchinnikov, W. Haase, *Chem. Mater.* **1996**, *8*, 922–926; c) K. Binnemans, Y. G. Galyametdinov, R. Van Deun, D. W. Bruce, S. R. Collinson, A. P. Polishchuk, I. Bikchantaev, W. Haase, A. V. Prosvirin, L. Tinchurina, I. Litvinov, A. Gubajdullin, A. Rakhmatullin, K. Uytterhoeven, L. Van Meervelt, *J. Am. Chem. Soc.* **2000**, *122*, 4335–4344; d) V. S. Mironov, Y. G. Galyametdinov, A. Ceulemans, K. Binnemans, *J. Chem. Phys.* **2000**, *113*, 10293–10303; e) K. Lodewyckx, R. Van Deun, K. Binnemans, *Mater. Sci. Eng. C* **2001**, *18*, 217–221; f) R. Van Deun, K. Binnemans, *Mater. Sci. Eng. C* **2001**, *18*, 211–215; g) K. Binnemans, R. Van Deun, C. Görller-Walrand, W. Haase, D. W. Bruce, L. V. Malykhina, Y. G. Galyametdinov, *Mater. Sci. Eng. C* **2001**, *18*, 247–254; h) K. Binnemans, C. Görller-Walrand, *Chem. Rev.* **2002**, *102*, 2303–2345.
- [9] a) A. A. Knyazev, Y. G. Galyametdinov, B. Goderis, K. Driesen, K. Goossens, C. Gorller-Walrand, K. Binnemans, T. Cardinaels, *Eur. J. Inorg. Chem.* **2008**, 756–761; b) S. Tang, A. Babai, A.-V. Mudring, *Angew. Chem.* **2008**, *120*, 7743–7746; *Angew. Chem. Int. Ed.* **2008**, *47*, 7631–7634.
- [10] a) S. Suárez, O. Mamula, R. Scopelliti, B. Donnio, D. Guillon, E. Terazzi, C. Piguet, J. C. G. Bünzli, *New J. Chem.* **2005**, *29*, 1323–1334; b) E. Terazzi, S. Suárez, S. Torelli, H. Nozary, D. Imbert, O. Mamula, J. P. Rivera, E. Guillet, J. M. Benich, G. Bernardinelli, R. Scopelliti, B. Donnio, D. Guillon, J. C. G. Bünzli, C. Piguet, *Adv. Funct. Mater.* **2006**, *16*, 157–168; c) S. Kumari, A. K. Shingh, K. R. Kumar, B. Sridhar, T. R. Rao, *Inorg. Chim. Acta* **2009**, *362*, 4205–4211; d) C. Piguet, J. Claude, G. Bunzli, B. Donnio, D. Guillon, *Chem. Commun.* **2006**, 3755–3768; e) S. Kumari, A. K. Singh, T. R. Rao, *Mater. Sci. Eng. C* **2009**, *29*, 2454–2458; f) C. V. Yelamaggad, R. Prabhu, G. Shanker, D. W. Bruce, *Liq. Cryst.* **2009**, *36*, 247–255; g) V. I. Dzhabarov, A. A. Knyazev, M. V. Strelkov, E. Yu. Molostova, V. A. Schustov, W. Haase, Y. G. Galyametdinov, *Liq. Cryst.* **2010**, *37*, 285–291; h) A. Escande, L. Guenee, E. Terazzi, T. B. Jensen, H. Nozary, C. Piguet, *Eur. J. Inorg. Chem.* **2010**, 2746–2759; i) T. B. Jensen, E. Terazzi, K.-L. Buchwalder, L. Guenee, H. Nozary, K. Schenk, B. Heinrich, B. Donnio, D. Guillon, C. Piguet, *Inorg. Chem.* **2010**, *49*, 8601–8619; j) T. B. Jensen, E. Terazzi, B. Donnio, D. Guillon, C. Piguet, *Chem. Commun.* **2008**, 181–183.
- [11] Yu. G. Galyametdinov, G. I. Ivanova, I. V. Ovchinnikov, *Bull. Acad. Sci. USSR Div. Chem. Sci. (Engl. Transl.)* **1991**, *40*, 1109–1116.
- [12] a) K. Binnemans, K. Lodewyckx, *Angew. Chem.* **2001**, *113*, 248–250; *Angew. Chem. Int. Ed.* **2001**, *40*, 242–244; b) R. Van Deun, K. Binnemans, *Liq. Cryst.* **2001**, *28*, 621–627; c) K. Binnemans, K. Lodewyckx, B. Donnio, D. Guillon, *Chem. Eur. J.* **2002**, *8*, 1101–1105; d) M. Marcos, A. Omenat, J. Barbera, F. Duran, J. L. Serrano, *J. Mater. Chem.* **2004**, *14*, 3321–3327; e) K. Binnemans, K. Lodewyckx, T. Cardinaels, T. N. P. Vogt, C. Bourgogne, D. Guillon, B. Donnio, *Eur. J. Inorg. Chem.* **2006**, 150–157; f) Y. T. Yang, K. Driesen, P. Nockemann, K. Van Hecke, L. Van Meervelt, K. Binnemans, *Chem. Mater.* **2006**, *18*, 3698–3704.
- [13] a) H. Miwa, N. Kobayashi, K. Z. Ban, K. Ohta, *Bull. Chem. Soc. Jpn.* **1999**, *72*, 2719–2728; b) J. Z. Li, H. Xin, M. Li, *Liq. Cryst.* **2006**, *33*, 913–919.
- [14] a) C. Piechocki, J. Simon, J. J. André, D. Guillon, P. Petit, A. Skoulios, P. Weber, *Chem. Phys. Lett.* **1985**, *122*, 124–128; b) J. Sleven, C. Görller-Walrand, K. Binnemans, *Mater. Sci. Eng. C* **2001**, *18*, 229–238; c) F. Maeda, K. Hatsusaka, K. Ohta, M. Kimura, *J. Mater. Chem.* **2003**, *13*, 243; d) K. Binnemans, J. Sleven, S. De Feyter, F. C. De Schryver, B. Donnio, D. Guillon, *Chem. Mater.* **2003**, *15*, 3930–3938; e) A. G. Gürek, T. Basova, D. Luneau, C. Lebrun, E. Kol'tsov, A. K. Hassan, V. Ahsen, *Inorg. Chem.* **2006**, *45*, 1667–1676.
- [15] I. Bikchantaev, Y. G. Galyametdinov, O. Kharitonova, I. V. Ovchinnikov, D. W. Bruce, D. A. Dunmur, D. Guillon, B. Heinrich, *Liq. Cryst.* **1996**, *20*, 489–492.
- [16] T. Cardinaels, K. Driesen, T. N. Pa rac-Vogt, B. Heinrich, C. Bourgogne, D. Guillon, B. Donnio, K. Binnemans, *Chem. Mater.* **2005**, *17*, 6589–6598.
- [17] Y. G. Galyametdinov, L. V. Malykhina, W. Haase, K. Driesen, K. Binnemans, *Liq. Cryst.* **2002**, *29*, 1581–1584.
- [18] a) K. Binnemans, B. Gundogan, *J. Rare Earths.* **2002**, *20*, 249–255; b) S. Suárez, O. Mamula, D. Imbert, C. Piguet, J. C. G. Bünzli, *Chem. Commun.* **2003**, 1226–1227.
- [19] a) C. R. Bhattacharjee, G. Das, P. Goswami, P. Mondal, S. K. Prasad, D. S. S. Rao, *Polyhedron* **2011**, *30*, 1040–1047; b) M. Pietraszkiewicz,

- S. Mal, O. Pietraszkiewicz, *Opt. Mater.* **2012**, *34*, 1507–1512; c) L. Guo, G. Hu, W. Li, S. Zhang, *SIFCD*. **2012**, *2*, 48–52.
- [20] B. Keshavan, P. G. Chandrashekara, N. M. Made Gowda, *J. Mol. Struct.* **2000**, *553*, 193–19.
- [21] T. Chattpadhyay, M. Mukherjee, K. S. Banu, A. Banerjee, E. Suresh, E. Zangrando, D. Das, *J. Coord. Chem.* **2009**, *62*, 967–979.
- [22] a) B. L. An, M.-L. Gong, M.-X. Li, J.-M. Zhang, *J. Mol. Struct.* **2004**, *687*, 1–6; b) M. D. Regulacio, M. H. Publico, J. A. Vasquez, P. N. Myers, S. Gentry, M. Prushan, S.-W. T. Chang, S. L. Stoll, *Inorg. Chem.* **2008**, *47*, 1512–1523.
- [23] J. A. Fernandes, R. A. S. Ferreira, M. Pillinger, L. D. Carlos, I. S. Gonçalves, P. J. A. R.-Claro, *Eur. J. Inorg. Chem.* **2004**, 3913–3919.
- [24] a) G. Barberio, A. Bellusci, A. Crispini, M. Ghedini, A. Golemme, P. Prus, D. Pucci, *Eur. J. Inorg. Chem.* **2005**, 181–188; b) G. Johansson, V. Percec, G. Ungar, D. Abramic, *J. Chem. Soc. Perkin Trans. 1* **1994**, 447–459; c) R. M. Richardson, S. A. Ponomarenko, N. I. Boiko, V. P. Shibaev, *Liq. Crys.* **1999**, *26*, 101–108; d) M. Marcos, R. Giménez, J. L. Serrano, B. Donnio, B. Heinrich, D. Guillou, *Chem. Eur. J.* **2001**, *7*, 1006–1013; e) V. Percec, G. Johansson, J. Heck, G. Ungarb, S. V. Battyb, *J. Chem. Soc. Perkin Trans. 1* **1993**, 1411–1420; f) V. Percec, D. Tomazos, J. Heck, H. Blackwell, Goran Ungar, *J. Chem. Soc. Perkin Trans. 2* **1994**, 31–44; g) X. Cheng, F. Su, R. Huang, H. Gao, M. Prehm, C. Tschierske, *Soft Matter* **2012**, *8*, 2274–2285; h) T. Shimogaki, S. Dei, K. Ohta, A. Matsumoto, *J. Mater. Chem.* **2011**, *21*, 10730–10737.
- [25] a) D. Pucci, I. Aiello, A. Bellusci, A. Crispini, I. D. Franco, M. Ghedini, M. La Deda, *Chem. Commun.* **2008**, 2254–2256; b) E. Terazzi, S. Torelli, G. Bernardinelli, J.-P. Rivera, J.-M. Bénech, C. Bourgogne, B. Donnio, D. Guillou, D. Imbert, J.-C. G. Bünzli, A. Pinto, D. Jeannerat, C. Piguet, *J. Am. Chem. Soc.* **2005**, *127*, 888–903; c) M. Stepien, B. Donnio, J. L. Sessler, *Chem. Eur. J.* **2007**, *13*, 6853–6863.
- [26] a) M. Douglas, N. M. Kroll, *Ann. Phys.* **1974**, *82*, 89–155; b) D. D. Koelling, B. N. Harmon, *J. Phys. C* **1977**, *10*, 3107–3114; c) C. Lee, W. Yang, R. G. Parr, *Phys. Rev. B* **1988**, *37*, 785–789; d) B. Delley, *J. Chem. Phys.* **1990**, *92*, 508–517.

Received: May 1, 2013

Revised: June 23, 2013

Published online: August 12, 2013